Scanning tunneling microscope instrumentation

Y. Kuk and P. J. Silverman

Citation: Rev. Sci. Instrum. **60**, 165 (1989); doi: 10.1063/1.1140457
View online: http://dx.doi.org/10.1063/1.1140457
View Table of Contents: http://rsi.aip.org/resource/1/RSINAK/v60/i2
Published by the American Institute of Physics.

REVIEW ARTICLE

Scanning tunneling microscope instrumentation

Y. Kuk and P. J. Silverman

AT&T Bell Laboratories, Murray Hill, New Jersey 07974

(Received 11 July 1988; accepted for publication 21 October 1988)

A review is presented of the basic operating principles of scanning tunneling microscopy and spectroscopy. The physical and electronic design of the scanning tunneling microscope is discussed, and other new microscopes using similar concepts are described. Some examples of the past accomplishments of scanning tunneling microscopy are given, and prospects for future applications are assessed.

INTRODUCTION

The understanding of surface structure has been a major concern of condensed matter physics and chemistry. Surface structures have been studied by conventional electron microscopes [e.g., transmission electron microscope (TEM) and scanning electron microscope (SEM)], diffraction measurements [e.g., low energy electron diffraction (LEED), x-ray, He diffraction], and scattering experiments (e.g., ion scattering). Direct imaging of geometric and electronic surface structures with atomic resolution had been a dream until the invention of scanning tunneling microscopy by Binnig, Rohrer, and co-workers[1] in 1981. Since the observation of the real-space image of Si(111)-(7×7),[2] a structure which had been an unresolved problem for more than 20 years, scanning tunneling microscopy has been accepted as a powerful surface science tool. Each of the microscopes developed earlier than the scanning tunneling microscope (STM) (Fig. 1) has certain strengths and limitations. The resolution of the optical microscope and SEM is not good enough to image surface atoms. High-resolution TEM, which has been used mainly for bulk and interface imaging, can reveal surface structures of specially thinned samples. The field emission microscope (FEM) and field ion microscope (FIM) probe the two-dimensional geometry of the atomic structure only on the surface of sharp tips with radius < 1000 Å.

There already exist several review articles[4-7] devoted to scanning tunneling microscopy. The main purpose of this article is to provide a comprehensive account of the STM as an instrument. Before presenting the various aspects of instrumentation, the principle of tunneling microscopy will be briefly explained. Following this, details of STM design will be discussed, including vibration isolation and electronics. Other instruments developed from the operating principles of scanning tunneling microscopy will then be introduced. Finally, a few examples will be given to demonstrate the advantages of scanning tunneling microscopy.

A. Principles of STM

In scanning tunneling microscopy, the three-dimensional variation of the charge density at a surface is probed via electron tunneling between a sharp tip and the sample. This vacuum tunneling phenomenon has been known since the introduction of quantum mechanics in the 1920's.[8,9] One-dimensional planar tunneling has been often used as an idealized model to describe three-dimensional vacuum tunneling.[10,11] From the solution of a one-dimensional barrier with plane waves,[12] the tunneling current can be written

$$I = c/d^2\{(\bar{\phi} - eV/2)\exp[-A(\bar{\phi} - eV/2)^{1/2}d] - (\bar{\phi} + eV/2)\exp[-A(\bar{\phi} + eV/2)^{1/2}d]\}, \quad (1)$$

where $A = 1.025(\text{eV})^{-1/2}$ Å^{-1}, $\bar{\phi}$ is the average of the barrier height between the two electrodes, V is the bias potential between the sample and the tip, and c is a constant. Equation (1) is valid even when the gap voltage V is > 5 V, in the field emission regime. When the gap is small and the voltage low, the current–gap distance relation can be simplified to

$$I \propto (V/d)\exp(-A\bar{\phi}^{1/2}d). \quad (2)$$

Equation (2) indicates that a 1-Å change in the gap distance produces roughly an order of magnitude change of the tunnel current with $\bar{\phi} \sim 4$ eV. This exponential dependence was measured by Young *et al.*[9,13] and Teague[14] and later by Binnig *et al.*[1] Young *et al.* realized that surface structures could be mapped by using a feedback system to maintain a constant tunneling current. This early device, called the topo-

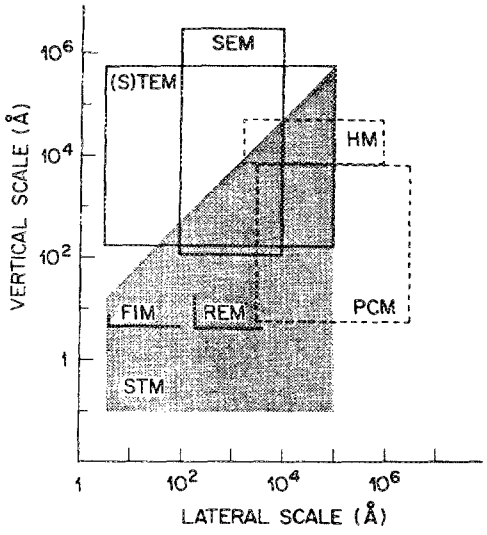

FIG. 1. Comparison of the range of resolutions of the STM and other microscopes. HM: high-resolution optical microscope. PCM: phase contrast microscope. (S)TEM: (scanning) transmission electron microscope. SEM: scanning electron microscope. FIM: field ion microscope. (See Ref. 3.)

 0034-6748/89/020165-16$01.30

grafiner, had an x–y–z scanning piezoelectric driver and constant current feedback, but it failed to give atomic resolution, perhaps due to insufficient vibration isolation and the large gap distance used (100–1000 Å). The scanning device of Binnig and Rohrer had good vibration isolation and stable feedback and was maintained under UHV conditions, resulting in unprecedented resolution of surface atoms.

Figure 2 shows a schematic diagram of a STM. When a bias voltage is applied between tip and sample, electrons can tunnel through the vacuum gap of ~10 Å. The feedback loop which controls the tunneling gap maintains a constant tunneling current and hence a fixed gap distance. (The relationship between gap and current is actually more complex as we will discuss below but this is a good starting approximation.) As the tip is scanned laterally across the surface by the x–y driver, changes in the z-piezo driver voltage reflect changes in the surface height.

Some three-dimensional tunneling theories have been developed from the transfer Hamiltonian approach.[15,16] In this approach, the tunneling barrier is treated as a perturbing Hamiltonian, in which two sides (tip and sample) are regarded as two independent systems with weak coupling. The net current can then be described by

$$I \sim \int_{-\infty}^{\infty} dE \rho_s(E+eV)\rho_t(E) \times |M(E)|^2 [f(E) - f(E+eV)], \quad (3)$$

where M is the tunneling matrix element, $f(E)$ is the Fermi function and ρ_s, ρ_t are the densities of states in the sample and the tip, respectively. Several groups have used Eq. (3) to derive the tunneling current,[17–22] a formidible task. Since the tunneling current is proportional to the convolution of the electronic states of sample and tip, and if the tip can be approximated as a hemisphere with s wave function, the tunneling current can be simplified in the low-voltage limit[17] to

$$I \propto V \rho_s(\mathbf{r}_0; E_F)\rho_t(E_F), \quad (4)$$

where $\rho_s(\mathbf{r}_0; E_F)$ is the surface density of states of the sample at the center of the tip ($\mathbf{r}_0$) and $\rho_t(E_F)$ is the density of states of the tip at the Fermi level. (ρ_t is often regarded as a constant.) This relation shows that the tunneling tip follows a contour of constant local density of surface states. At low voltage, only the states near the Fermi levels of the sample and the tip contribute to the tunneling current.

As the bias voltage is finite ($\bar{\phi} > V > 1V$), the relation should be modified to[23]

$$I \propto \int_0^{eV} \rho(E) D(E,V) dE, \quad (5)$$

where $\rho(E)$ is sample surface density of states and $D(E,V)$ is the transmission coefficient of the barrier at voltage V. D can be calculated by the WKB method or by Eq. (1); the result is shown in Fig. 3. The measured image is, therefore, a function of bias voltage, due to the energy dependence of the surface density of states. With appropriate bias, the sign of eV in Eq. (5), both filled and empty states can be measured. Lang has shown that when scanned by an atomically sharp tip, the observed size of a surface atom is a function of gap voltage due to the density of states.[20] For these reasons, it is necessary to take images at several gap voltages in order to gain a comprehensive picture of the surface structure.[24]

B. Scanning tunneling spectroscopy

A normal STM image contains both geometric and electronic information about the surface. The electronic information can also be separately measured.[25,26] With the tunneling tip poised over a region of interest and the gap fixed by opening the feedback loop momentarily, the bias voltage can be ramped (e.g., from -3 to $+3$ V) to measure the tunneling current as a function of applied voltage. This measurement can be performed at each point of a topography scan, resulting in spatially resolved $I(V)$ relations. Some electronic structural information, such as the energy-band gap of semiconductors or superconductors, can be directly obtained. In the low bias voltage limit, the local density of states can be deduced[22] from dI/dV (differential conductance) vs V by

$$dI/dV \propto \rho(r,V)D(V), \quad (6)$$

where $\rho(r,V)$ is the local density of states of the sample eval-

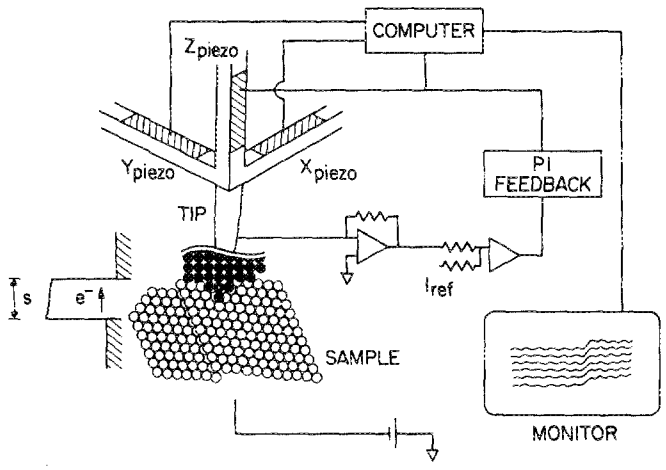

FIG. 2. Schematic diagram of a STM. A voltage is applied across the gap and the resultant tunneling current is fed back to the z piezo to maintain the current constant. The measured error signal is proportional to the corrugation as the tip is scanned laterally.

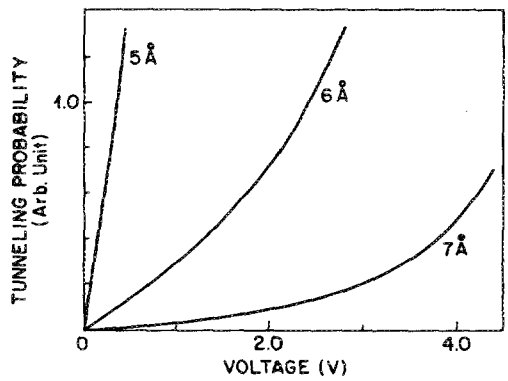

FIG. 3. The tunneling probability as a function of the gap voltage and the gap distance, calculated by the WKB method. For a (100 Å)^2 planar junction, 1.0 on y axis indicates 1-nA tunneling current.

uated at the center of the tip (r), and $D(V)$ is defined in Eq. (5). dI/dV vs V has been shown to be proportional to the density of states in the low-voltage limit in metal–insulator–metal tunneling.[10] A plot of $d \ln I/d \ln V$ vs V[23] removes the exponential shape of $D(V)$, and the peaks in this curve correspond roughly to resonances in the tip and sample densities of states, although their exact heights and positions also depend on the gap distance.[21,27]

Since the area probed by the STM is typically so small, the uncertainty principle may play a role in determining the energy resolution of this spectroscopy. Assuming that the radius and the lateral resolution of a tunneling tip are roughly equal, the relation $\Delta k \Delta x \sim 1$ indicates that a tip of radius 2 Å will have a momentum uncertainty of 0.5 Å^{-1}. (Although the crystal momentum in a solid is not a physical momentum, a resolution limit can be estimated.) In Fig. 4 (a), showing the energy-band structure of nearly free electrons in a periodic potential, a sharp tip is indicated by the heavy line spanning the first and the second Brillouin zone; poor momentum resolution results in poor energy resolution around the probing energy V_g. The broken line in the figure indicates the better momentum and energy resolution attained with a dull tip. Figure 4 (b) depicts the measured densities of states using dull and sharp tips for a two-band model of nearly free-electron dispersion. For a sharp tip, the measured density of states does not reveal detailed structure due to its poor energy resolution. A sharp tip, therefore, is desirable for topographic scanning but undesirable for tunneling spectroscopy on a surface with a dispersive band structure.[28]

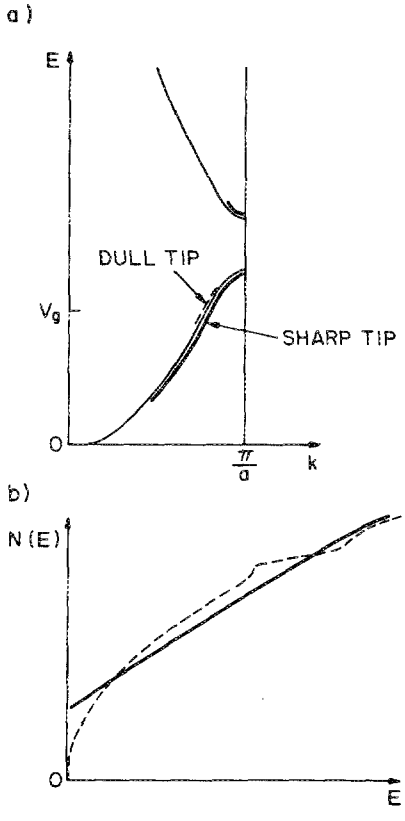

FIG. 4. Band structure of nearly free-electron dispersion for a two-band model. The band structure along k perpendicular direction is shown in (a) with energy resolution. The measured densities of states for a dull tip (broken line) and a sharp tip (solid line) are shown.

I. DESIGNS

A. Vibration

The exponential dependence of the tunneling current on gap distance makes vibration isolation an extremely critical factor in good STM design. The basic concepts of vibration isolation have been treated in several textbooks[29,30] and papers.[31–33] For many surfaces, especially metals, the atomic corrugations observed in a constant current STM scan will typically be 0.1 Å, so one must set a vibration isolation goal of ~0.01 Å or less. (Even better vibration isolation may be required for the detection of inelastic tunneling signals.[34])

There are two types of disturbance from which a STM must be isolated: vibration and shock. Vibrations are generally repetitive and continuous. A typical floor vibration spectrum on the fourth floor in AT&T Bell Laboratories is shown in Fig. 5. Low-frequency floor vibration (1–3 Hz) is appreciable; vibrations at ~8, 29, and 60 Hz originated from ventilation ducts, motors, and transformers, respectively. Shock is defined as a transient condition whereby kinetic energy is transferred to a system in a short time period. The isolation of shock will not be discussed, but an excellent review can be found in the literature.[29]

Figure 6 shows a simplified form of a vibration isolation system. When the floor of a laboratory vibrates with known amplitude with respect to a reference frame, the vibration amplitude on top of the vibration isolation system (Fig. 6) with respect to this frame can be calculated. For a spring and a viscous damping system, the resulting vibration amplitude transfer can be described by

$$T = \left(\frac{1 + (2\xi\nu/\nu_n)^2}{(1 - \nu^2/\nu_n^2)^2 + (2\xi\nu/\nu_n)^2} \right)^{1/2}, \tag{7}$$

where ν is the external excitation frequency, ν_n is the resonance frequency, $\xi (= \gamma/\gamma_c)$ is the damping ratio, γ is the damping coefficient of the system, and $\gamma_c (= 4m\pi\nu_n)$ is the critical damping coefficient. Figure 7 shows a family of amplitude transfer curves for the system shown in Fig. 6.

Various materials can be used for the spring and viscous damping components. Organic materials, including rubber and Viton, can be used, but they exhibit pronounced creep. They are most effective against large amplitude shock, and

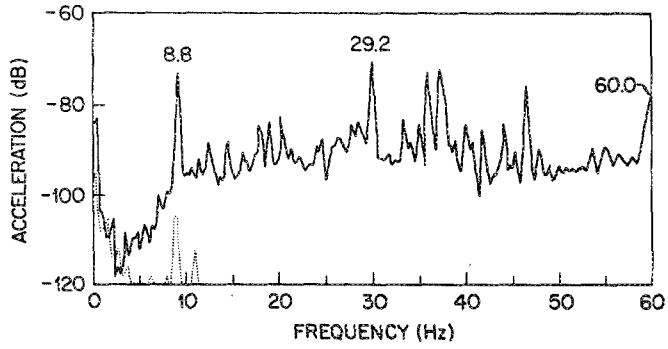

FIG. 5. The vibration spectrum of the floor in the authors' laboratory. (Solid line) vibrations are reduced on a commercial air spring table (dotted line).

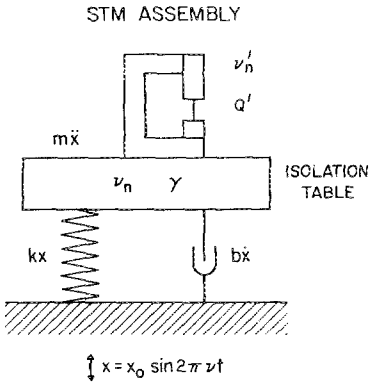

FIG. 6. Block diagram of a STM system on vibration isolation system. The isolation system is simplified to a spring and a viscous damper. The STM assembly has its own structural damping.

are substantially incompressible (Poisson's ratio ~ 0.5). When strained under compression (e.g., the Viton spacers separating the five stacked metal plates used in IBM Zurich's "pocket STM" isolator[35]), their compression stiffness (equivalent to the spring constant) is often large, resulting in a rather high (>10–100 Hz) resonance frequency. However, they have inherent damping, depending on the material, in the range of 0.05–0.3 times the critical damping. Metal springs, on the other hand, can have smaller spring constants, yielding low resonance frequencies (as low as 0.5 Hz), but they provide little damping and require additional damping components. Though viscous damping is used in many vibration isolation schemes, magnetic eddy current damping is more widely used in UHV STMs because of its vacuum compatibility and its easily varied damping coefficient. The eddy current damping coefficient γ (in g/s) can be written as

$$\gamma = 9.69\times 10^{-9} B^2 l S/\rho, \tag{8}$$

where B is the magnetic field in gauss, l is the thickness (in the direction of B) of the conductor (cm), S is the cross-sectional area (cm^2), and ρ is the resistivity in Ω cm. In general, eddy current damping using permanent magnets is useful only if the mass and the natural frequency of the system are relatively low. Commercially available vibration isolation systems employing pneumatic springs are often used as the support for a STM. With a surge tank and capillary flow resistance, these can have a resonance frequency as low as 0.5 Hz and a variable damping constant. Figure 5 shows the dramatic reduction (>60 dB at 10 Hz), produced by a commercial system in our laboratory.

A rigidly constructed STM does not require many stages of vibration isolation.[36,37] Vibrations are dissipated by hysteresis loss due to the inherent structural damping of a rigid body. The damping transfer function for hysteresis loss, equivalent to amplitude transfer, is given by

$$T^S = \frac{(\nu/\nu_n')^2}{[(1-\nu^2/\nu_n'^2)^2 + (\nu/\nu_n' Q')^2]^{1/2}}, \tag{9}$$

where ν_n' is the resonance frequency and Q' is the quality factor of the tip–sample junction. Piezo drivers with resonance frequencies up to 100 kHz can be constructed, but other factors, such as joints tightened by screws, epoxy junctions, three-point contacts, walker resonance, and loose spring connectors often reduce this to 1–5 kHz for the junctions of many actual STM units. For a system with one stage vibration isolation and structural damping with $\nu_n' \gg \nu_n$, the resultant transfer function can be expressed by

$$T_{\text{total}} = \left(\frac{1+(\xi\nu/\nu_n)^2}{(1-\nu^2/\nu_n^2)^2 + (2\xi\nu/\nu_n)^2}\right)^{1/2} \times \frac{(\nu/\nu_n')^2}{[(1-\nu^2/\nu_n'^2)^2 + (\nu/\nu_n' Q')^2]^{1/2}}. \tag{10}$$

The amplitude transfers for four STMs are shown in Fig. 8. The solid line is for a system with $\nu_n = 2$ Hz, $\nu_n' = 2$ kHz,

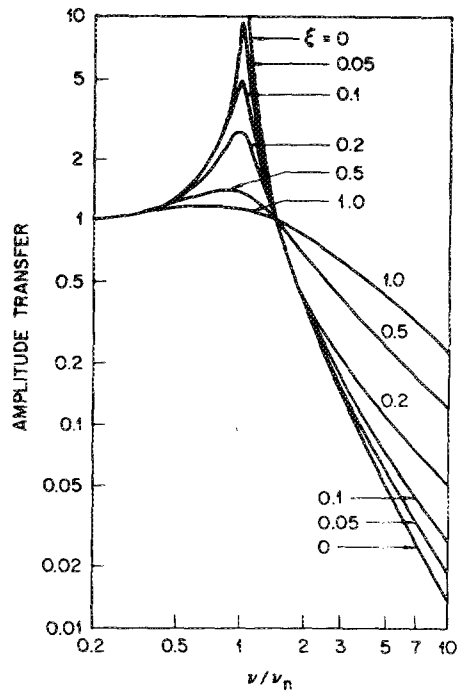

FIG. 7. Amplitude transfer of one-stage vibration isolation as a function of frequency and damping ratio (from Ref. 30).

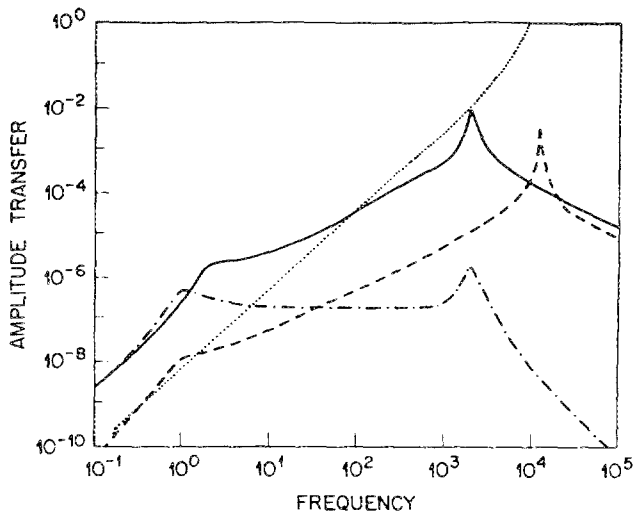

FIG. 8. Total amplitude transfer for four systems with different vibration isolations and structural dampings (see text).

$\zeta = 0.4$, and $Q' = 10$. With a floor vibration amplitude of a few thousand Å, the gap stability for this system will be worse than 1 Å (not stable enough). For a very rigid STM assembly (shown as a dotted line in Fig. 8 where $\nu_n' = 12$ kHz and $Q' = 50$), the amplitude transfer is still too large (worse than 1 Å at 200 Hz) for a stable STM junction. With the addition of a vibration isolation table ($\nu_n = 1$ Hz and $\zeta = 0.4$), the amplitude transfer (shown as a broken line) is $< 10^{-6}$ and the tunneling gap will be stable to < 0.01 Å at 200 Hz. The fourth case (shown as a chained line — - - —) is for a system in our laboratory with two-stage vibration isolation: one by an internal spring system ($\nu_n = 1$ Hz, $\zeta = 0.4$) and another by an external table ($\nu_n = 1.1$ Hz, $\zeta = 0.5$). The structural damping for the STM assembly is $\nu_n' = 2$ kHz and $Q' = 10$. In most of the frequency range, the estimated vibration amplitude is less than 0.001 Å.

B. Mechanical designs

There are several criteria to be satisfied in the design of an ideal STM. Basic goals for construction are a high mechanical resonance frequency and a low Q factor for the tip driver and sample holder as described above, an x–y scanning range of $\sim 1\ \mu$ with accuracy of ~ 0.1 Å, and a z scanning range of 1 μ with ~ 0.01-Å resolution. The means of reducing the gap distance to within z-piezo range, known as the sample coarse approach system, should be smooth without rocking motion or backlash, in order to avoid an accidental contact with the tunneling tip, and should move with < 0.1-μ accuracy.

PZT [Pb(Ti, Zr)O_3] is a piezoelectric ceramic widely used as an electromechanical transducer to obtain the x–y–z motion and the sample coarse approach. Electromechanical properties of various piezoelectric ceramics can be found elsewhere.[38–41] PZT ceramics are available in a variety of shapes and configurations from many manufacturers, including Vernitron (UK and USA), Tokin (Japan), Siemens (Germany), and Edo Western (USA). The primary concern in their use is the distortion of the resultant STM images due to their hysteresis, creep, and thermal drift.[42]

The first x–y–z tip driver built by Young *et al.* consisted of two x–y piezo tubes and a stacked z-piezo driver.[13] A tripod design of three orthogonal piezo"sticks" with high-resonance frequency, permitting high-resolution scanning, was developed by Binnig and his co-workers.[1] Replacement of the "sticks" by tubes reduces the cross talk and raises the resonance frequency.[43,44] A compact, single tube scanner, first designed by Germano[45] and later by Binnig and Smith,[46] has recently become popular. This design, Fig. 9, exhibits large displacements, low cross talk, and high resonance frequency. The resonance frequency in Hz of the single tube design can be estimated by

$$f_r = 1.08 \times 10^5 [(r_0^2 + r_i^2)^{1/2}/l^2], \qquad (11)$$

where r_i, r_0 are the radius of the inner wall and outer wall, respectively, and l is the length of the tube in cm. Designs employing separate tube drivers for tip and sample or using many symmetrically arranged piezo blocks have been successful in reducing the effects of thermal drift.[47–49]

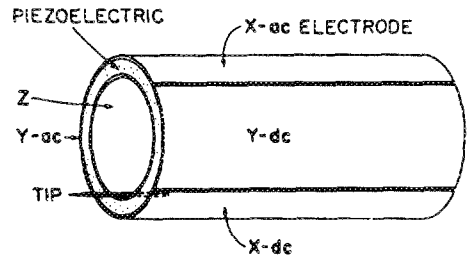

FIG. 9. Schematic diagram of a single tube x–y–z scanner (from Ref. 47).

Three designs for the sample approach being used by many groups are: (1) a walker ("louse") which moves by using electrostatic, mechanical, or magnetic[50–53] clamping and piezo expansion (similar to a commercial "inchworm"[54]), (2) a differential screw micrometer pushing on a reduction lever, and (3) a micrometer pushing against a differential spring. Walkers have been widely used in UHV chambers.[35,43,44,47,55–60] A typical design of this type is shown in Fig. 10. The walker consists of a piezoelectric plate and dielectric feet to which the clamping voltages are applied. A variety of dielectric materials, including $SrTiO_3$, BN, thin slide glass, Al_2O_3, and PZT have been used for the feet. Some walker designs perform unreliably due to their high sensitivity to the surface condition of the dielectric material; poor clamping results in a low resonance frequency. Lever or differential screw mechanisms have been used[61–68] for fast approach and easy manipulation of the sample holder, which can usually be detached or flipped away from the STM assembly. Two representative designs by Demuth *et al.*[61] and Drake *et al.*[67] are shown in Figs. 11(a) and 11(b). The motion of a lead screw, turned by rotational manipula-

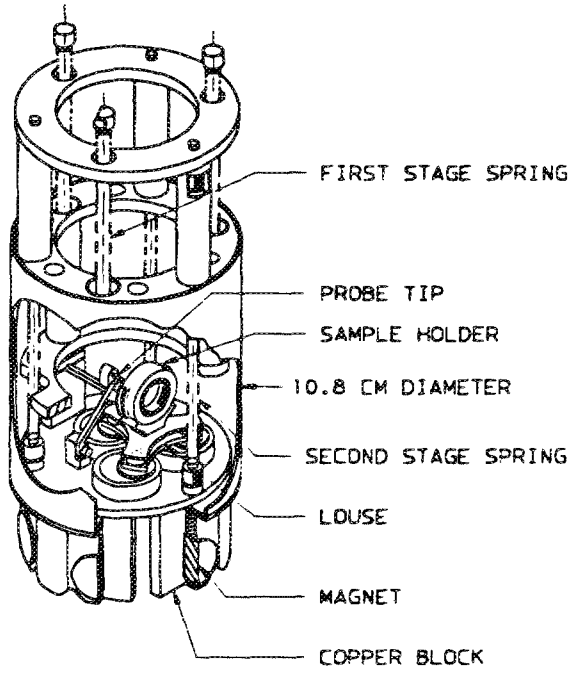

FIG. 10. Schematic diagram of STM by R. M. Feenstra *et al.* (see Ref. 56). Double-stage isolation system with springs and eddy current assembly is shown. A "louse" used for sample coarse approach and a tripod x–y–z piezo driver are visible.

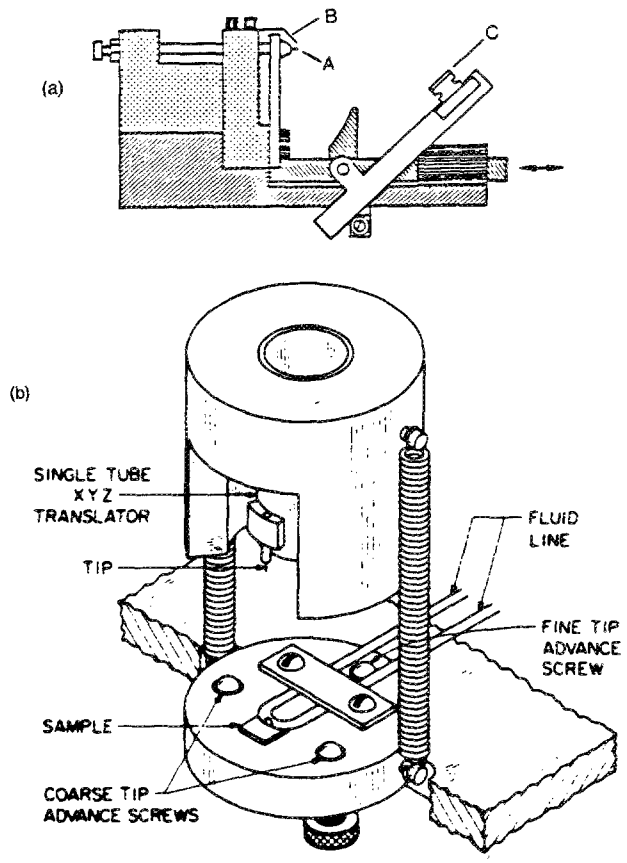

FIG. 11. (a) Schematic diagram of STM by Demuth *et al.* (see Ref. 62). Letters are explained in the reference. (b) Schematic diagram of STM by Drake *et al.* (see Ref. 68). Liquid can be supplied through the fluid line.

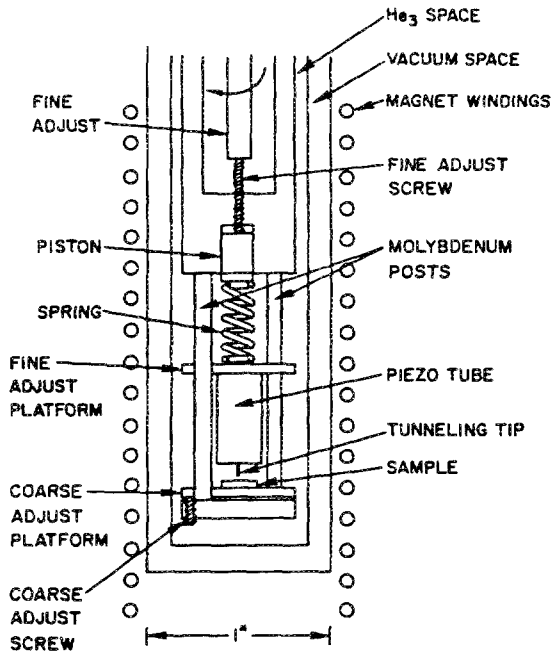

FIG. 12. Cross-sectional schematic of low-temperature STM by Fein *et al.* (Ref. 70), utilizing a differential spring for coarse approach and a tube scanner.

tor, is reduced by a lever with a ratio of 1/100–1/5000, resulting in a 500-Å to 25-μ translation per revolution. Some commercially built STMs use this design.[63,68] Problems occasionally arise from a bistable joint position or roughness of the lead screw, which can cause sudden large movements. The differential spring mechanism[69-73] is quite similar to a lever-type design (Fig. 12); the reduction of motion is produced by the difference in spring constants between two springs. In principle, either design can achieve a high resonance frequency.

Several groups have built special purpose STMs. Electrochemistry can be studied by a system with a liquid supply line.[67,74] STMs have been built under an optical microscope to locate macroscopic objects.[75,76] Some groups[77,78] have constructed small STMs to understand light interaction with the tunneling junction, e.g., frequency mixing and asymmetric junction characterization. Relatively few STMs which operate at low temperature, in order to study superconducting states, phonons, and molecular vibrations,[10,11,79] have been built to date. The mechanical design of such an instrument represents a considerably greater challenge because of the problems of stability, dimensional contraction, and reduced piezoelectric response under cryogenic conditions. The first type developed was simply a compact STM directly immersed in liquid N_2 or He.[80,81] Next, a very small STM was designed which could be placed in a tube evacuated by a turbomolecular or ion pump, and the tube inserted into an He^4 or He^3 Dewar. In this scheme, a rigid construction with resonance frequency > 50 kHz is necessary for adequate vibration isolation. Figure 12 shows the schematic diagram of the low-temperature STM of Fein *et al.*[69] While most of these STMs do not have the capability of *in situ* sample cleaning, Eigler[82] has constructed one with a transferable sample holder to permit sputtering and annealing. In a third type of STM, the assembly is in contact with a reservoir of liquid He^4 (or N_2) inside an UHV chamber equipped with standard surface characterization tools.[83,84] Since a rather large STM assembly must be cooled by thermal conduction, temperature stability is difficult, resulting in large thermal drifts.

C. Electronics

Since the STM is a subangstrom servo device, the electronic design should be closely coupled to the mechanical design. Information on automatic controls[85,86] and circuit designs for STMs[32,51,64,87-89] can be found elsewhere. Before the circuit is designed, a feedback circuit analysis should be performed. The motion to be controlled by negative feedback is schematically shown in Fig. 13. In a constant current scan, the gap separation is set by comparing the tunneling current to the demand current and is regulated by a negative feedback loop. The response function of each component in Laplace transformation is given by the following relations:

$$G_1(s) = k_p/(s\tau_p + 1) \quad (12a)$$

$$G_2(s) = k_i/(s\tau_i + 1) \quad (12b)$$

$$G_3(s) = k_{hv}/(s\tau_{hv} + 1) \quad (12c)$$

$$H_1(s) = \omega_n^2 k_t/(s^2 + \omega_n s/Q + \omega_n^2) \quad (12d)$$

$$H_2(s) = k_l/(s\tau_l + 1), \quad (12e)$$

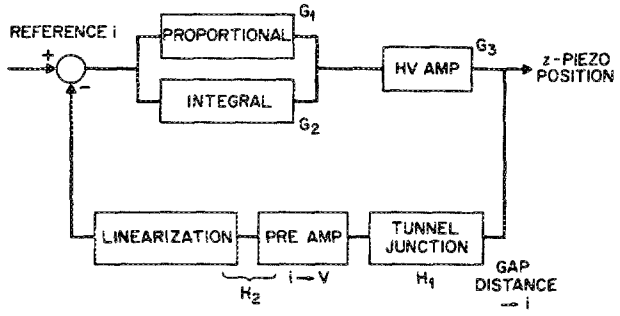

FIG. 13. Block diagram of STM negative feedback control system. Linearization can be obtained with or without logarithmic amplifier. The transfer functions of each part are described in Eq. (12).

where G_1, G_2, G_3 are the transfer functions of the proportional feedback (subscript p), the integral feedback (subscript i) and the high-voltage amplifier (subscript hv), respectively. H_1 and H_2 are the transfer functions of the tunneling gap and the preamplifier (including logarithmic amplifier if there is one), respectively. k and τ stand for the gain and the time constant of each system. The resonance frequency and the Q factor of the tunneling gap can be measured experimentally. Although the settling time of a feedback system can be shortened with a proportional feedback component, $k_p = 0$ for many existing STMs. The resultant transfer function $T(s)$ for the feedback system shown in Fig. 13 can be written by

$$T(s) = \frac{[G_1(s) + G_2(s)]G_3(s)}{1 + [G_1(s) + G_2(s)]G_3(s)H_1(s)H_2(s)}, \qquad (13)$$

where response functions are given by Eq. (12). For the authors' STM at AT&T Bell Labs using a walker and tripod x–y–z piezo design with $\omega_n \sim 1.2\times10^4$, $Q\sim10$, $\tau_I \sim 3\times10^{-4}$, and $\tau_I \sim 0.11$, the transient response of the feedback system, calculated from Eq. (13), is shown in Fig. 14. Three cases with three different loop gains are shown. The response is overdamped with a gain of 100, critically damped with 200, and underdamped with 1000.

Once the gain is set (200 in this case), the circuit can be designed. The frequency response of the feedback system can be derived from Eq. (13) by replacing s by $i\omega$ to get the Bode diagram.[85] A typical block diagram of a feedback circuit is shown in Fig. 15. The tip voltage can be supplied by a battery or computer DAC. The tunneling current can then be measured by a preamplifier with a gain of 10^6–10^9 V/A. (Princeton Applied Research, Keithley, and Ithaco make such preamplifiers.) The signal can then be linearized by a logarithmic amplifier (e.g., Burr Brown 4271 or Analog Devices 755) to improve the dynamic range. When a flat surface is scanned, the logarithmic amplifier is not necessary and a linear approximation of the exponential dependence of the tunneling current can be used. The measured tunneling current is compared with the demanded current, and the resultant error signal is fed into the main feedback amplifiers, consisting of an analog integrator with variable time constant and a proportional amplifier. (This part can be replaced by digital feedback, but analog feedback is faster than most ADC–DAC combinations at present.) The feedback signal is then applied to the z-piezoelectric driver. (The Kepco BOP series is often used, but home-built circuits are also popular.) For the x–y piezos, separate high-voltage amplifiers controlled by DACs or synchronized ramp generators are used. The computer used for STM control and data acquisition should thus have at least two ADC channels and four DACs. Since the feedback is a high gain circuit, electrical noise and pickup can be a problem in some environments; shielding of signal and control wires, however, may introduce undesirable capacitive effects. In addition, the STM has its own intrinsic noise which is little understood.

A sample and hold amplifier, inserted in the circuit just ahead of the proportional and integral amplifiers, permits the measurement of the I vs V characteristic at constant gap distance; conductance as a function of x–y position[24–26] can also be measured in this way. During the hold period, the error signal is set to zero so that the z-piezo voltage does not change, maintaining a fixed tunneling gap. The tip voltage can be varied at the same time, and the resulting current can be measured by ADC. This I vs V relation gives information about the electronic structure of the surface as described earlier.

When the tip is scanned faster then the feedback can respond (above the crossover frequency in the Bode diagram), the feedback loop gain will be smaller than 1, and the signal applied to the z piezo cannot follow the topography of the surface. If the response of the preamplifier of the system is still faster than the scanning speed, the measured tunneling current reflects the surface topography. This method, known as fast scanning,[90] works well on a flat surface like graphite, but surface roughness could result in accidental contact of the tip with the sample.

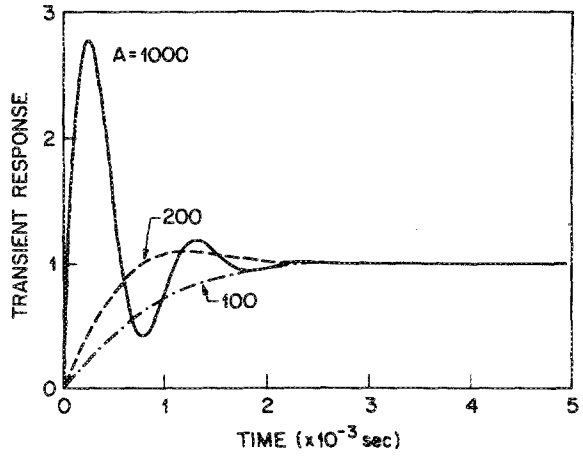

FIG. 14. Transient response of the STM control system in Fig. 13. The results for three different loop gains are shown.

D. Tunneling tip

One of the major questions in scanning tunneling microscopy is the role played by the structure of the tunneling tip in any set of measurements. The size, shape, and chemical identity of the tip influence not only the resolution and shape of a STM scan but also the measured electronic structure. Experimentally, tips have been prepared by mechanical

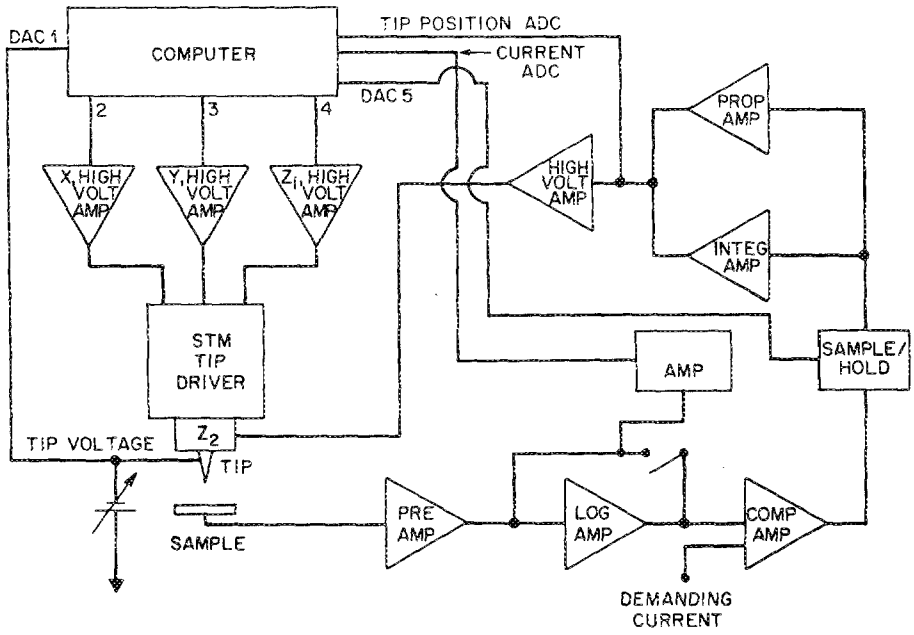

FIG. 15. Block diagram of STM feedback circuit based on circuit analysis.

grinding or electrochemical etching from a variety of materials, most often W. Since a bcc crystal has lower surface energy on the (110) faces, ⟨100⟩ and ⟨111⟩, oriented tips (single-crystal wires) can be sharpened by annealing in the presence of a high electric field,[43,91,92] producing a pyramid shape of (110) facets. When tip annealing capability and high electric field are not available, a high tunneling current (100 nA–10 μA) is known to either clean or sharpen the tunneling tip. These techniques are supposed to produce a sharp, clean, and symmetric tip, but asymmetric or double tips are often formed, resulting in misleading sample topographs.

Only one experiment has been reported[43] in which a tunneling tip with known geometry was used to image a surface structure. By taking the FIM image of the tunneling tip before and after a STM scan, the character of the STM topograph can be correlated to the tip structure. The dependence of the measured corrugation amplitude on the size of the tunneling tip was experimentally examined. Figure 16 (a) shows a FIM picture of the tunneling tip used in the STM scan of the clean Au(001)–(5×1) surface with corrugation width of 14.4 Å [Fig. 16 (b)]. The corrugation amplitude was estimated theoretically[17] as

$$\Delta \propto \exp[-\beta(R+d)], \tag{14}$$

where $\beta \simeq (1/4)\kappa^{-1}G^2$. R is the radius of curvature of the tip (approximated as a hemisphere), d is the gap distance, κ^{-1} is the electron decay length in the vacuum, and G is the smallest surface reciprocal wave vector ($2\pi/a_i$, and a_i is the largest corrugation width). Figure 17 shows average measured corrugations of the Au(100)–(5×20) and the Au(110)–(1×2) reconstructions[93] as a function of the tip size. The measured β's for the Au(100) and Au(110) are in good agreement with the values predicted by Eq. (14). Tip size versus measured corrugation for several other surfaces is shown. Two broken horizontal lines in Fig. 17 indicate STM noise levels, due typically to mechanical vibration or electronic noise, for two hypothetical STMs. The significance of the tip size is now apparent from Fig. 17. For a noise level corresponding to 0.5 Å, the tip must be terminated by a single atom in order to detect any reconstruction. On the other hand, the corrugations of the Au(100), Au(110), and Si(111)–(7×7) surfaces could be detected by a 20-Å tip, with a STM noise level of 0.05 Å. Most metal surfaces with small reconstruction unit cells or (1×1) surfaces require a very sharp tip and low STM noise level, making atomic resolution difficult to achieve without special treatment of the tunneling tip.

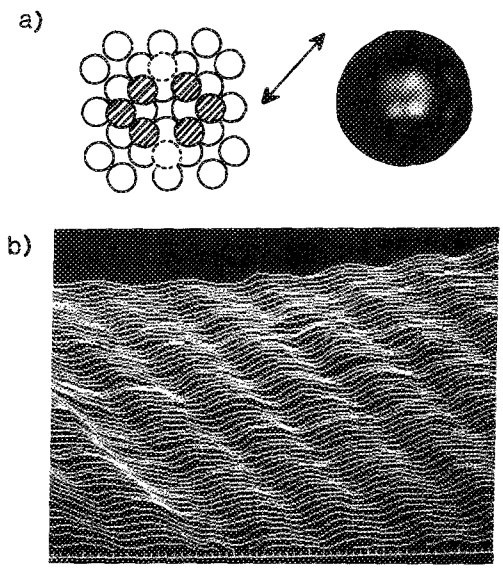

FIG. 16. (a) FIM image of the W(100) tip before and after the STM scan. The arrow indicates the scanning direction with respect to the tip. Filled circles are the first layer atoms. (b) STM topograph of Au(001). Rows along the close-packed ⟨1$\bar{1}$0⟩ are separated by ~14 Å. Scales along the (1$\bar{1}$0), (110), and (001) indicate 10, 10, and 2 Å, respectively.

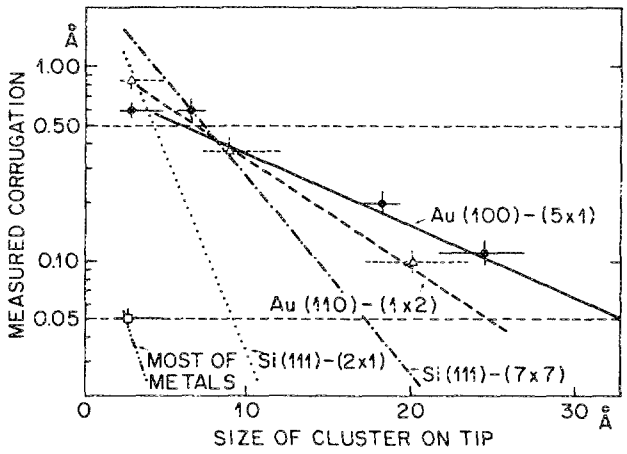

FIG. 17. Dependence of measured corrugation on size of tip for Au(001)-(5×1) (solid line and filled circle), Au(110)-(1×2) (broken line and triangle), Si(111)-(7×7) (— · —), Si(111)-(2×1) (dotted line), and most metals without reconstruction (— · · —).

E. Sample preparation

Preparation of a flat, clean, well-ordered surface is as important as having a sharp tunneling tip in attaining high-resolution topographs. For example, in an UHV STM, well-ordered areas are sometimes difficult to find even when the LEED pattern of the surface shows sharp diffraction spots with low background. For many surfaces, a sharp LEED pattern is a necessary but not sufficient condition for successful STM imaging. Ideally, the sample surface should have large well-ordered domains and few impurities, and should exhibit roughness no more than a few atoms in height, in order to avoid accidental contact of the tip.

Most surfaces examined under UHV conditions can be cleaned and ordered by annealing alone or by sputtering and annealing. A well-ordered Si(111)-(7×7), used as the *de facto* standard for STM calibration, can usually be obtained by high-temperature annealing only; ion sputtering often leaves many defects on the surface. Some semiconductor reconstructions examined by STM have been on cleaved,[55] laser annealed,[94] MBE deposited, and capped surfaces.[66] Metals seldom show many vacancies due to sputtering damage, so repeated sputtering/annealing cycles result in clean, well-ordered surfaces with large domain sizes.[93] Graphite surfaces have been widely studied in the air,[95] in liquids,[96] and in UHV. This surface, like other layered structure materials, can be prepared by cleaving.

II. OTHER MICROSCOPES

Several related scanning microscopes have been developed since the invention of the STM: atomic force microscope (AFM),[97] scanning tunneling potentiometry (STP),[98] scanning near field optical microscope (SNOM),[99] scanning capacitance microscope,[100] ballistic electron emission microscope (BEEM),[101] and tracking tunneling microscope.[102] This section will be devoted to only brief descriptions of the operational principles of a few of these; details can be found in the listed references.

A. Atomic force microscope

The AFM was invented by Binnig, Quate, and Gerber in 1986.[97] It is capable of measuring extremely small interatomic forces.[103-106] Unlike STM, AFM permits the study of nonconducting materials. In AFM, a constant force balanced by a mechanical spring is maintained between a tip (diamond,[107] tungsten, or SiO_2[108]) and the sample surface. A simple order-of-magnitude calculation yields a value of 1 eV/1 Å ($= \sim 10^{-9}$ N) for the interatomic force between atoms on the sample and the tip. The spring constant of the balancing spring should therefore be the same as the force gradient, 10^{-9} N/Å (= 10 N/m). Such springs have been made from a variety of materials, including thin wires[107] and thin foils by microfabrication.[108,109] The mass must be small in order to make the resonance frequency, $2\pi\sqrt{k/m}$, high enough (2–3 kHz) to have rigid body damping against external vibrations.

Various schemes have been used to maintain the constant force feedback[97] (Fig. 18). In the method most widely used at present, the tunneling current measured by a STM from the back of the stylus is used to maintain the constant current feedback for the STM and constant force feedback for AFM. The STM part can be replaced by a capacitance measurement probe for a low resolution measurement. This method has produced atomic resolution on surfaces of layered materials.[105,107,108,110] The position of the stylus can also be measured optically, making the instrument sensitive to both attractive and repulsive forces. Since the absolute position of the stylus against the tip is measured by interference between two optical paths,[111] thermal drift presents a problem. Optical heterodyne detection[106] has been used to measure the change of the resonance frequency in the presence of van der Waals forces. In this case, the change of amplitude, which is proportional to the gap distance, is used to maintain a constant value of the AFM force.

B. Scanning tunneling potentiometry

STP was developed to understand electron transport through condensed matter.[91] It not only measures the topo-

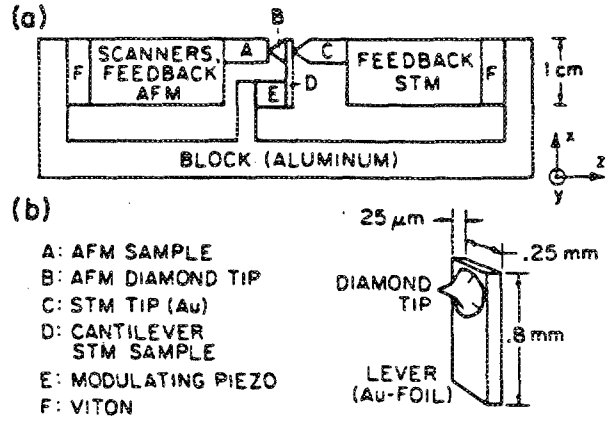

FIG. 18. Block diagram of AFM by Binnig *et al.* (Ref. 91). The size of the cantilever is not in scale. A diamond tip is scanning the sample A and the position of the lever is detected by tunneling between the back of the lever and the STM tip C.

graphy of surfaces but also the electric potential distributions, giving an insight into conduction through granular structures, defects, and interfaces. STP requires a minor modification of a STM: two additional electrodes on the surface. A dc potential is applied across the sample surface, while an ac voltage applied across the tunneling gap provides an ac tunneling current which can be used to maintain the tunneling gap constant. The measured dc voltage gives the local potential at the scanning position. Recent results show the possibilities for understanding the conduction mechanism through junctions.[112,113]

C. Scanning near field optical microscope

The resolution of a conventional optical microscope is limited by the wavelength of visible light. A way to improve this resolution was first proposed by Ash and co-workers[114] and developed by Durig *et al.*,[92] Fisher *et al.*,[115] and Lewis *et al.*[116] The basic principle of SNOM is that electromagnetic fields can be enhanced at curved parts of a surface. Light can be transmitted through and reflected from an aperture as small as $\lambda/25$. Since the energy density changes with distance and dielectric constant beyond the aperture, the transmitted and reflected light intensity varies with the topography and composition of the sample. The gap between the aperture and the surface can be regulated by electron tunneling current, using the principle of scanning tunneling microscopy. Although its resolution (~ 200 Å) is not as good as STM, it has great potential to study not only surface topography but also optical interactions on a microscopic scale.

III. EXAMPLES AND FUTURE

A. Semiconductor surfaces

One of the most notable achievements of scanning tunneling microscopy has been the elucidation of the atomic arrangements of semiconductor surfaces. Despite a great deal of experimental and theoretical effort, it was only with the availability of the STM and its direct imaging capability that significant progress was made in resolving the detailed structure of the Si(111)–(7×7).[2,117–120] Binnig, Rohrer, and their co-workers showed that 12 adatoms are present in a (7×7) unit cell with charge-density minima at the corners. Becker *et al.*[117] found that the (7×7) reconstruction persists undistorted right up to an atomic step in the surface (Fig. 19), suporting the dimer-adatom-stacking fault model by Takayanagi.[121] Hamers *et al.*[118,119] have reported on the correlation of the geometric and electronic surface structures. By combining scanning tunneling microscopy and spectroscopy, they identified surface states with specific atomic sites. Figure 20 shows the tunneling spectroscopy current images of occupied Si(111)–(7×7) adatom, dangling, and backbond states. Tromp *et al.*[122] have performed a scanning tunneling microscopy study of the Si(001)–(2×1) reconstruction (Fig. 21). It was observed that only symmetric dimers form the basic structure of the Si(001)–(2×1), while buckled dimers are often seen near surface defects. By tunneling at different bias voltages, they were able to image the charge density of the filled and empty

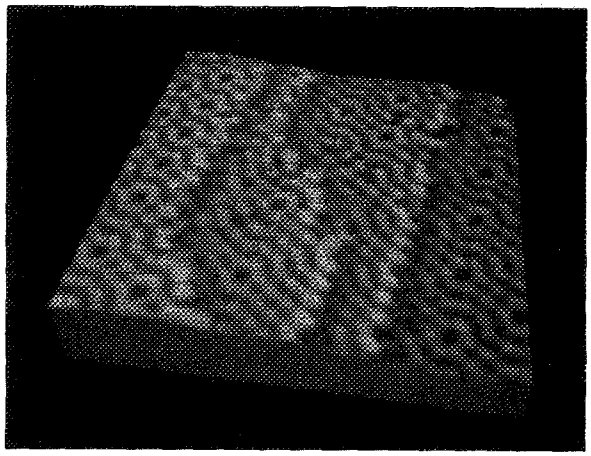

FIG. 19. STM image of the Si(111)–(7×7) with 12 adatoms in a unit cell. Figure from R. Becker.

states. Other groups have studied the reconstruction of the cleaved Si surface or high Miller index surfaces.[123,126]

Feenstra *et al.* first demonstrated the atom-selective imaging power of scanning tunneling microscopy on the GaAs(110)–(1×2) surface[23] by using the difference in lateral positions of state-density maxima between occupied and unoccupied states (Fig. 22). As a result, either Ga atoms or As atoms were imaged, depending on the bias voltage. By comparing the measured images with theoretical predictions, the buckling angle of the Ga and As bonds were estimated. This is one of the few cases in which STM data were used to determine the vertical position of surface atoms.

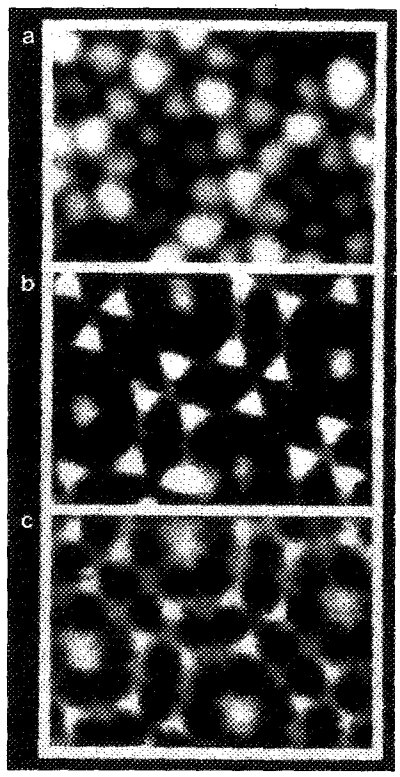

FIG. 20. Current imaging tunneling spectroscopy images of occupied states of the Si(111)–(7×7): (a) adatom state at −0.35 V, (b) dangling bond state at −0.8 V, (c) backbond state at −1.7 V. Figure from R. J. Hamers.

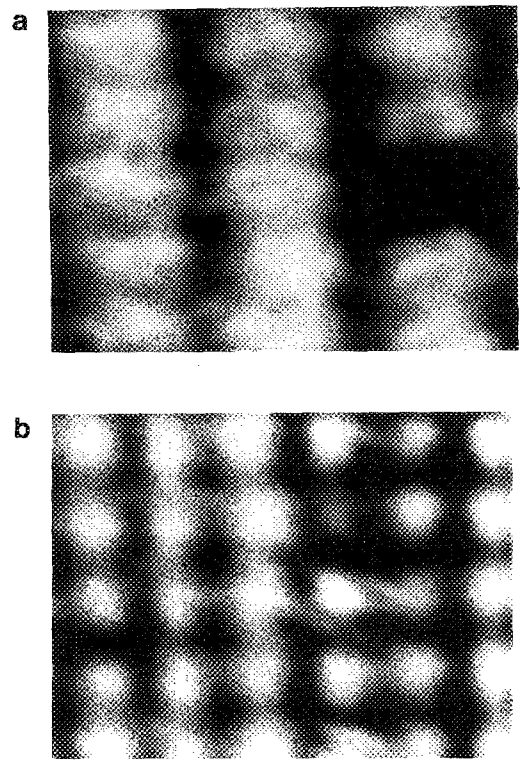

FIG. 21. Constant current images of the Si(001)-(2×1) taken simultaneously at (a) + 1.2 V and (b) − 2 V. Filled and empty state images show charge transfer in dimers. Figure from R. J. Hamers.

Chemisorption of oxygen on GaAs(110) has been studied by the same group.[126] They observed a long-range screening of the adsorbed atoms in the surrounding bare surface region.

In all of the cases described above, the STM provided information on the atomic arrangements of reconstructions. More recently, behavior of metallic overlayers, including Ag, Ni, Al, As, and In on the Si(111) surface has been studied by several groups.[127-132] Many of these overlayers show a metal/Si(111)-$(\sqrt{3}\times\sqrt{3})$R30 structure. Wilson and Chiang, e.g., showed the registry of the overlayer on the partially covered surface of Ag/Si(111). They have determined that Ag atoms are located at the honeycomb centers (H_3 sites) as shown in Fig. 23. From the coverage and annealing time dependence, the nucleation and dynamics of the overlayers were described.

B. Metal surfaces

Metal surfaces have been somewhat neglected by the STM community, perhaps because their preparation sometimes requires more rigorous conditions than for other materials; the shallow corrugations displayed by metals also require the STM to have high lateral and vertical resolution for atomic imaging (see Fig. 16). The Au(110)-(1×2) surface was first studied by Binnig, Rohrer, and their co-workers[133] and later by the authors' group.[134] The topograph (Fig. 24) shows (1×2) reconstruction with alternate $\langle 1\bar{1}0\rangle$ missing rows, in agreement with other experimental results. The observed ordered domain size also agrees with the broadening of the fractional order spots in LEED measurements.

Hallmark *et al.* imaged the Au(111)-(1×1) surface with atomic resolution in air and under UHV (Fig. 25).[135]

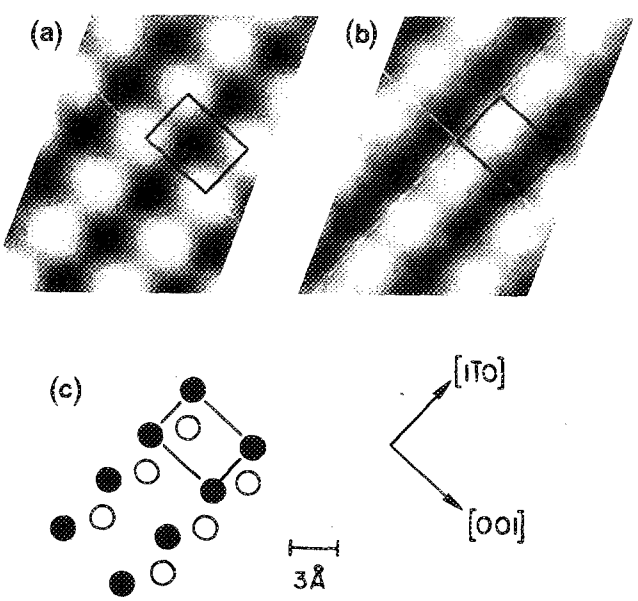

FIG. 22. Constant current images of GaAs(110) taken simultaneously at (a) 1.9 V and (b) − 1.9 V. Positions of surface atoms are schematically shown (c), where open circles indicate As atoms and closed circles are Ga atoms. Figure from R. M. Feenstra.

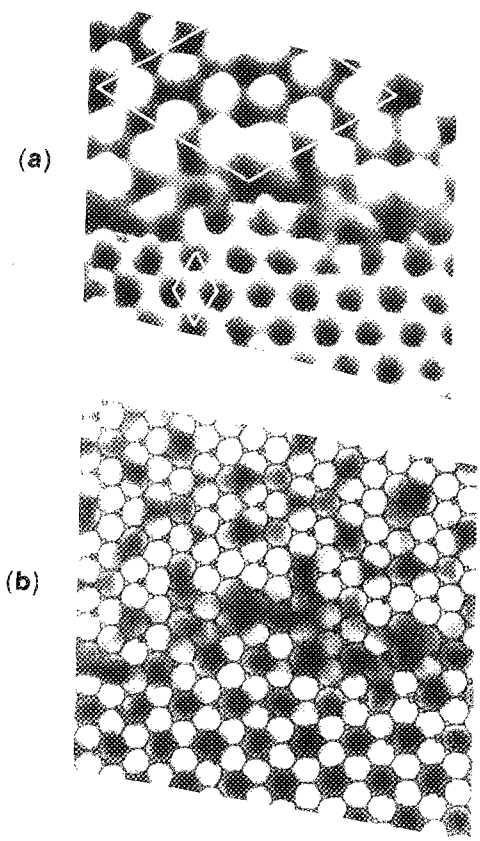

FIG. 23. Constant current images of a domain boundary between Si(111)-(7×7) and Si(111)-Ag-$(\sqrt{3}\times\sqrt{3})$R30°. (a) Perspective view with (7×7) and $(\sqrt{3}\times\sqrt{3})$ unit cells. (b) Top view with Si(111) mesh superimposed, showing the registry of Ag atoms. Figure from S. Chiang.

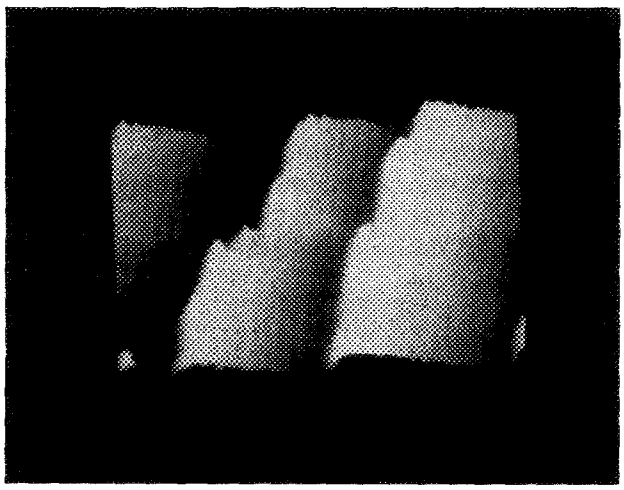

FIG. 24. Constant current image of the Au(110)–(1×2). Three terraces are shown with average terrace width of ~100 Å.

The high resolution and large corrugations observed by them were attributed to the existence of a surface state near the Fermi level. Recently, the authors' group also imaged individual atoms on the Au(100)–(5×20) reconstruction.[136] In this case, the unusually high spatial resolution and large corrugations were believed to be the result of foreign atoms picked up on the tip during scanning.

High spatial resolution (nearest-neighbor atoms separated by 2.5 Å) has also been attained on the hydrogen adsorbed Ni(110) surface[137] (Fig. 26). The topograph shows the local ordering of the (5×2) reconstruction; the small domain sizes observed are the result of a kinetics limited process at room temperature and agree with LEED observations. The local barrier height, measured simultaneously with the topograph, was found to be in agreement with macroscopic work function measurements.

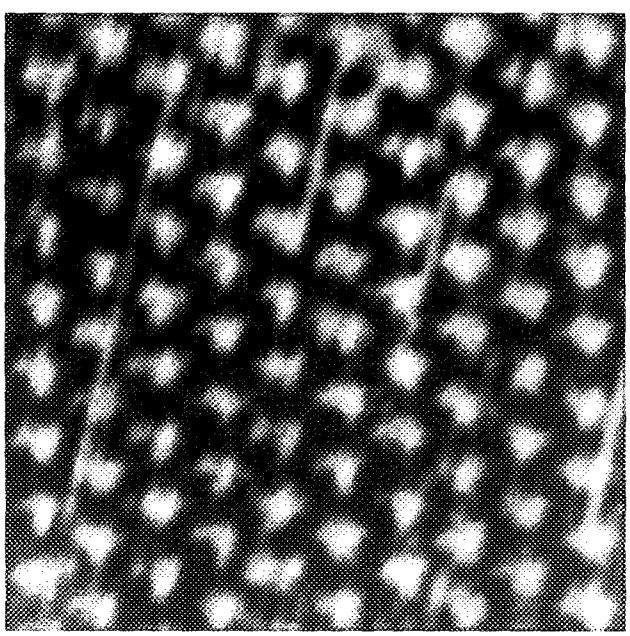

FIG. 25. Tunneling current image of the Au(111)–(1×1) in the air. Figure from S. Chiang.

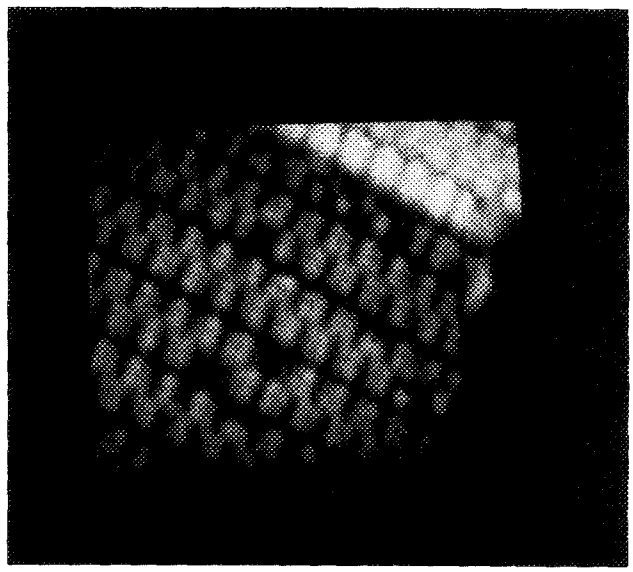

FIG. 26. Constant current image of the Ni(110)–H(5×2). Few defects including antiphase boundary and point defects are visible.

While most of the examples described above provide information on atomic arrangement of surface structure in equilibrium, a few studies have been performed on the dynamics or driving force responsible for structural transformation. Behm *et al.*[138] demonstrated that scanning tunneling microscopy can be used to study the dynamics of gas adsorption. Depending on adsorbates, nucleation sites were found either at steps or on terraces. The growth of adsorbates was observed as a function of exposure. Similarly, the structures formed by S on the Mo(100) surface[139] and the growth of Au layers on the Ni(110) surface were reported.[140]

C. Other surfaces

Graphite has been the most popular substrate for use with the STM since it can be easily cleaved to give a flat surface that can be imaged in air, liquid, or vacuum with atomic resolution.[87,88,141–146] There are, however, some puzzling aspects of the tunneling mechanism for graphite. When graphite is scanned in the constant current mode, giant corrugations (as large as 200 Å) are often observed. Soler *et al.*[145] attributed the effect to interatomic forces between tip and graphite. Even though this tunneling mechanism is not clearly resolved, graphite has been useful as a lateral scanning calibration standard and as a substrate for various adsorbates.

Other layered materials, such as the transition-metal chalcogenides, have been studied to understand charge-density waves on surfaces. While the charge densities of many surfaces probed by scanning tunneling microscopy resemble their atomic arrangements, this is not always true for materials exhibiting charge density waves. Figure 27 shows the charge-density waves of 4Hb–$TaSe_2$ at 4.2 K.[97,142,147] Two charge-density wave superlattices ($\sqrt{13}a_0 \times \sqrt{13}a_0$ in the 1-T sandwich and $3a_0 \times 3a_0$ in the 1-H sandwich) have been found to coexist on the same surface.

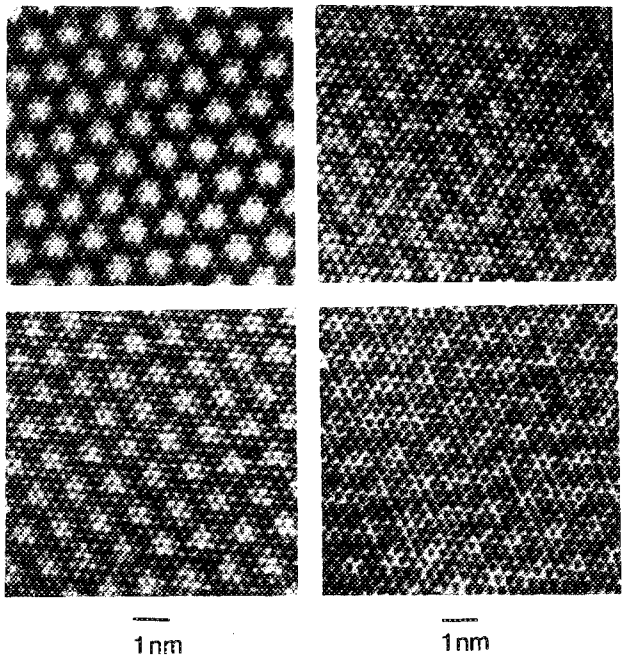

FIG. 27. Trigonal prismatic sandwich of 4Hb–$TaSe_2$ at 4.2 K. Different scans on same surface detect $\sqrt{13}a_0 \times \sqrt{13}a_0$ and $3a_0 \times 3a_0$ charge-density waves. Figure from R. V. Coleman.

A substantial effort has been made to image large organic or biological molecules. Conducting molecules and replicas (freeze-dried or metal layer coated) have been observed by scanning tunneling microscopy.[148-153] Sleator and Tycko imaged the topography of the conducting molecular crystal TTF–TCNQ. A well-ordered TTF–TCNQ surface is shown in Fig. 28, agreeing with the bulk crystal structure. The image was interpreted in terms of the molecular orbitals of TTF and TCNQ molecules. Figure 29 shows Pt–Ir–C coated recA–DNA complexes.[149] A large arrow indicates the recA–DNA complex and small arrows point to free DNA. Liquid crystals, which have order between crystalline and isotropic, were studied by Foster and Frommer (Fig. 30).[153] A nematic crystal, 4-(trans-4*n*-pentylcyclohexyl)

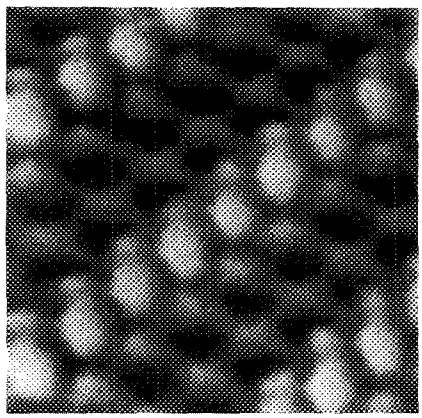

FIG. 28. Constant current image of TTF–TCNQ surface. The observed structure agrees well with the molecular structure. Figure from R. Tycko.

benzonitrile (5CBN), was imaged, showing a strong influence of the graphite substrate in determining the orientation of the crystal. Although at present the details of the tunneling mechanisms are lacking, the images of molecules confirm the potential of the STM in this field.

D. Applications

In many of the STM results described above, imaged areas were at most a few hundred Å on a side, since atomic resolution of the surface was of interest. This small field of view has limited the use of scanning tunneling microscopy on practical surfaces; finding a macroscopic structure is a formidable task at present. Recently, Gehrtz *et al.*[154] have constructed a STM capable of > 20-μ x–y motion and 4-μ z motion. Expanded range STMs such as this can be used for surface studies of technological problems on a larger scale; machined surfaces[154,155] and semiconductor microfabrication,[156] for example, can be imaged.

Lithography with a STM on a nanometer scale has been tried by various methods. McCord and Pease[157] made use of the scanning capability to draw 200-Å wide lines on a thin CaF_2 layer by a field emitted electron beam from the tunnel-

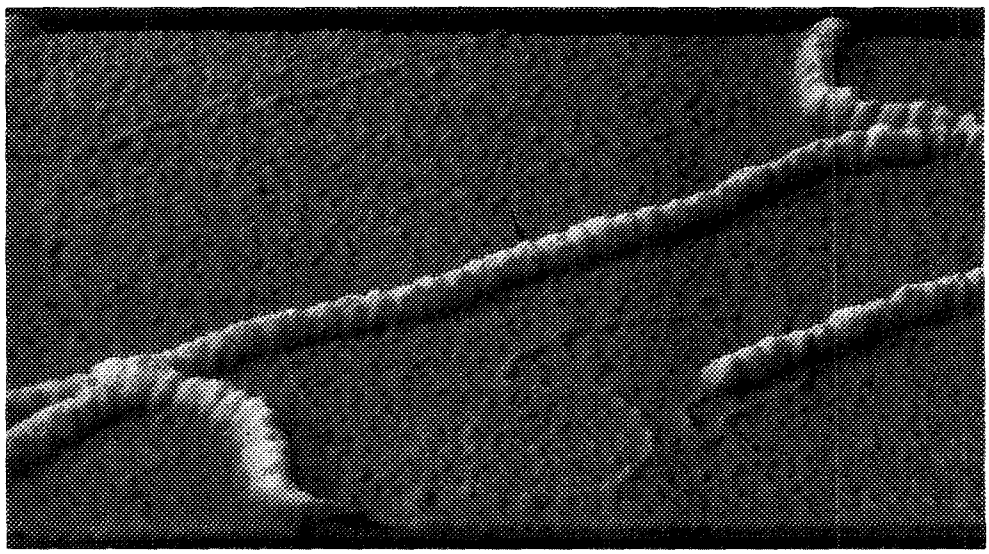

FIG. 29. 2360-Å × 1920-Å STM image of shadowed recA–DNA. Arrows indicate RecA–DNA and free DNA. Figure from G. Travaglini.

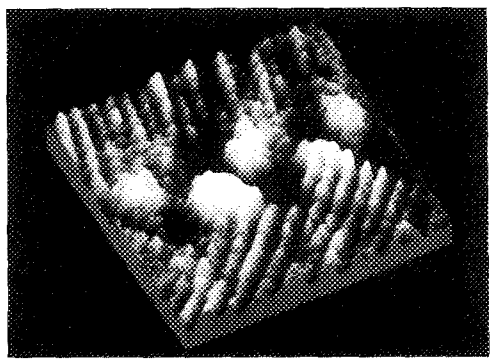

FIG. 30. Perspective view of the boundary between two orientations of 5CBN. (72 Å^2). Figure from J. S. Foster.

ing tip. Au surfaces were modified by applying a field of several V/Å in the tunneling gap, leading to possible nanofabrication of metal surfaces,[158] although surface diffusion[159] sets a limit for practical use. Figure 31 shows a spot created on a clean Ge(111) surface by raising the tip voltage to -4 V; an ensemble of such "nano-bits" could be used as a memory medium of extremely high density and storage capacity.[160]

The dynamics of chemical processes can be observed by STMs operating in liquids. Drake *et al.*[161] imaged the corrosion process of Fe film on an Al surface (Fig. 32). With the metal film and STM tip immersed in a saline solution, the corrosion process was imaged as a function of reaction time. Similar observations of Au electroplating onto a graphite surface were made by the same group.

E. Future

In its brief history, the STM has already become a powerful tool for the study of nanostructures in numerous areas of science and technology. Operation of a STM at high resolution is far from routine, however, and most published results are still obtained from home-built systems, despite the availability of several commercial instruments. The number of groups actively using STM is now in the hundreds and still rising rapidly, and many investigators are now buying ready-made equipment rather than building their own. It is hoped, then, that in the near future, there will be a gradual shift from unreliable instruments, with a low "duty cycle" of meaningful results, to STMs routinely usable by laboratory technicians, allowing researchers to concentrate on the physics of the surface of interest rather than on the instrument itself. The STM has already been brought to bear on problems in a wide variety of fields, but, as exciting as its development has been over the past few years, we have, figuratively and literally, "only scratched the surface."

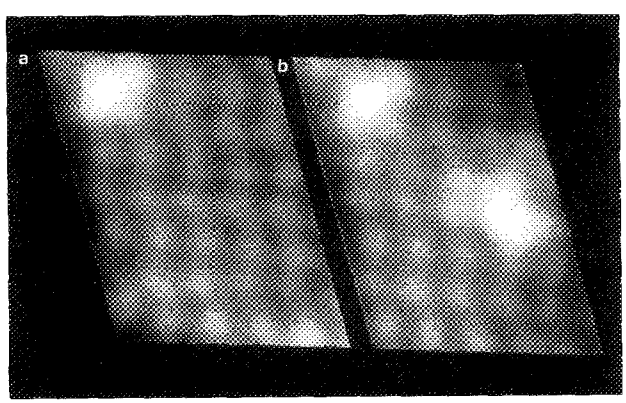

FIG. 31. Constant current image of a reconstructed Ge(111) surface prior to the modification (a) and after the modification (b).

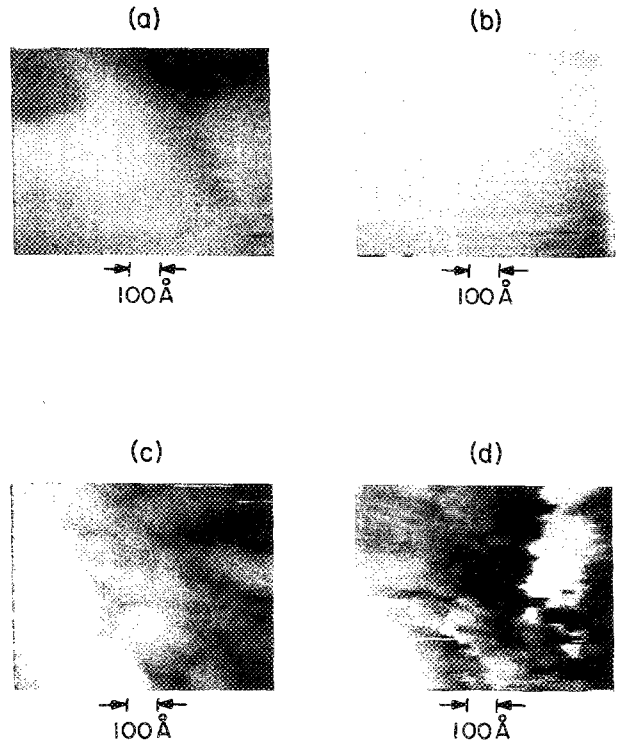

FIG. 32. STM images of a thin metal film (a) before the corrosion takes place, (b) after covered with a drop of saline solution, (c) 30 s after (b), and (d) 150 s after (c). Figure from P. K. Hansma.

ACKNOWLEDGMENTS

The authors thank W. L. Brown, H. Q. Nguyen, F. M. Chua, S. Foner, B. Ambrose, R. Becker, G. Binnig, P. J. Bryant, C. J. Chen, S. Chiang, R. V. Coleman, M. P. Cox, P. H. Cutler, P. Davisson, V. Eling, R. M. Feenstra, J. K. Gimzewski, J. E. Griffith, R. Guckenberger, H.-J. Guntherodt, D. R. Hamann, R. J. Hamers, P. K. Hansma, C. Heiden, H. F. Hess, R. C. Jaklevic, W. J. Kaiser, J. R. Kirtley, T. Klitsner, G. P. Kochanski, H. L. Krautwedel, R. McAllister, M. D. Pashley, D. W. Pohl, C. F. Qaute, H. Rohrer, T. Sakurai, T. Sleator, St. Tosch, G. Travaglini, I. S. T. Tsong, R. Tycko, and R. Wiesendanger.

[1]G. Binnig, H. Rohrer, Ch. Gerber, and E. Weibel, Appl. Phys. Lett. **40**, 178 (1982); Phys. Rev. Lett. **49**, 57 (1982); Physica **109/110b**, 2075 (1982).
[2]G. Binnig, H. Rohrer, Ch. Gerber, and E. Weibel, Phys. Rev. Lett. **50**, 120 (1983).
[3]G. Binnig and H. Rohrer, Helv. Phys. Acta **55**, 726 (1982).
[4]C. F. Quate, Phys. Today **26** (Aug 1986).
[5]P. K. Hansma and J. Tersoff, J. Appl. Phys. **61**, R1 (1987).

[6]T. E. Feuchtwang and P. H. Cutler, Phys. Scr. **35**, 132 (1987).
[7]G. K. Binnig and H. Rohrer, Rev. Mod. Phys. **59**, 615 (1987).
[8]R. H. Fowler and L. Nordheim, Proc. R. Soc. London **A119**, 173 (1928).
[9]R. D. Young, J. Ward, and F. Scire, Phys. Rev. Lett. **27**, 922 (1971).
[10]C. B. Duke, *Tunneling in Solids* (Academic, New York, 1969).
[11]E. L. Wolf, *Principles of Electron Tunneling Spectroscopy* (Clarendon, Oxford, 1985).
[12]J. G. Simmons, J. Appl. Phys. **34**, 1973 (1963).
[13]R. Young, J. Ward, and F. Scire, Rev. Sci. Instrum. **43**, 999 (1972).
[14]E. C. Teague, Ph.D. thesis, North Texas State University, 1978.
[15]J. Bardeen, Phys. Rev. Lett. **6**, 57 (1961).
[16]W. A. Harrison, Phys. Rev. **123**, 85 (1961).
[17]J. Tersoff and D. R. Hamann, Phys. Rev. Lett. **50**, 25 (1983); Phys. Rev. B **31**, 805 (1985).
[18]T. E. Feuchtwang, P. H. Cutler, and N. M. Miskovsky, Phys. Lett. **99A**, 167 (1983); M. S. Chung, P. H. Cutler, and T. E. Feuchtwang, Surf. Sci. **181**, 412 (1987).
[19]A. Baratoff, Physica **127B**, 143 (1984).
[20]N. D. Lang, Phys. Rev. Lett. **55**, 230 (1985); Phys. Rev. Lett. **56**, 1164 (1986); Phys. Rev. Lett. **58**, 45 (1987).
[21]C. J. Chen, J. Vac. Sci. Technol. A **6**, 319 (1988).
[22]A. Selloni, P. Carevali, E. Tosatti, and C. D. Chen, Phys. Rev. B **34**, 994 (1986).
[23]R. M. Feenstra, J. A. Stroscio, and A. P. Fein, Surf. Sci. **181**, 295 (1987).
[24]R. Feenstra, J. Stroscio, and A. P. Fein, Phys. Rev. Lett. **58**, 1192 (1987).
[25]R. J. Hamers, R. M. Tromp, and J. E. Demuth, Phys. Rev. Lett. **56**, 1972 (1986).
[26]R. S. Becker, J. A. Golovchenko, D. R. Hamann, and B. S. Swartzentruber, Phys. Rev. Lett. **55**, 2032 (1985).
[27]N. D. Lang, Phys. Rev. B **34**, 1164 (1986).
[28]R. Becker and R. M. Feenstra (private communication).
[29]*Shock and Vibration Handbook*, edited by C. M. Harris and C. E. Crede (McGraw-Hill, New York, 1976).
[30]R. W. Little, *Elasticity* (Prentice-Hall, Englewood Cliffs, New Jersey, 1973).
[31]S.-I. Park and C. F. Quate, Rev. Sci. Instrum. **58**, 2004 (1987).
[32]D. W. Pohl, IBM J. Res. Dev. **30**, 417 (1986).
[33]M. Okano, K. Kajimura, S. Wakiyama, F. Sakai, W. Mizutani, and M. Ono, J. Vac. Sci. Technol. A **5**, 3313 (1988).
[34]G. Binnig, N. Garcia, and H. Rohrer, Phys. Rev. B **32**, 1336 (1985).
[35]Ch. Gerber, G. Binnig, H. Fuchs, O. Marti, and H. Rohrer, Rev. Sci. Instrum. **57**, 221 (1986).
[36]P. K. Hansma, IBM J. Res. Dev. **30**, 396 (1986).
[37]G. Binnig and H. Rohrer, IBM J. Res. Dev. **30**, 355 (1986).
[38]W. G. Cady, *Piezoelectricity* (McGraw-Hill, New York, 1946).
[39]J. van Randeraat and R. E. Setterington, *PXE Piezoelectric Merumics* (Mullard, London, England, 1975).
[40]B. Jaffe, R. S. Roth, and S. Marzullo, J. Res. Natl. Bur. Stand. **55**, 239 (1955).
[41]W. R. Cook, D. A. Berlincourt, and F. J. Scholz, J. Appl. Phys. **34**, 1392 (1963).
[42]O. Nishikawa, M. Tomitori, and A. Minakuchi, Surf. Sci. **181**, 210 (1987).
[43]Y. Kuk and P. J. Silverman, Appl. Phys. Lett. **48**, 1597 (1986).
[44]S. Chiang and R. J. Wilson, IBM J. Res. Dev. **30**, 515 (1986).
[45]C. P. Germano, IRE Trans. **7**, 13 (1959).
[46]G. Binnig and D. P. E. Smith, Rev. Sci. Instrum. **57**, 1688 (1986).
[47]G. F. A. van der Walle, J. W. Gerritsen, H. van Kempen, and P. Wyder, Rev. Sci. Instrum. **56**, 1573 (1985).
[48]S. Gregory and C. T. Rogers, J. Vac. Sci. Technol. A **6**, 390 (1988).
[49]J. W. Lyding, S. Skala, R. Brockenbrough, J. S. Hubacek, and G. Gammie, Bull. Am. Phys. Soc. **33**, 319 (1988).
[50]B. W. Corb, M. Ringger, and H.-J. Guntherodt, J. Appl. Phys. **58**, 3947 (1985).
[51]K. Kajimura, H. Bando, K. Endo, W. Mitzutani, H. Murakami, M. Okano, S. Okayama, M. Ono, Y. Ono, H. Tokumoto, F. Sakai, K. Watanabe, and S. Wakiyama, Surf. Sci. **181**, 165 (1987).
[52]M. Anders, M. Thaer, and C. Heiden, Surf. Sci. **181**, 176 (1987).
[53]D. W. Pohl, Rev. Sci. Instrum. **58**, 54 (1987).
[54]Inchworm is commercially available from Burleigh Instruments, Inc., Fisher, New York.
[55]R. M. Feenstra, W. A. Thompson, and A. P. Fein, Phys. Rev. Lett. **56**, 608 (1986); J. Vac. Sci. Technol. A **4**, 1315 (1986).
[56]J. A. Golovchenko, Science **232**, 48 (1986).
[57]S. Chiang, R. J. Wilson, Ch. Gerber, and V. M. Hallmark, J. Vac. Sci. Technol. A **6**, 386 (1987).
[58]D. W. Abraham, H. J. Mamin, E. Ganz, and J. Clarke, IBM J. Res. Dev. **30**, 493 (1986).
[59]N. J. Zheng, U. Knipping, I. S. T. Tsong, W. T. Petuskey, and J. C. Barry, J. Vac. Sci. Technol. A **6**, 457 (1988).
[60]Th. Berghaus, H. Neddermeyer, and St. Tosch, IBM J. Res. Dev. **30**, 520 (1986).
[61]J. E. Demuth, R. J. Hamers, R. M. Tromp, and M. E. Welland, IBM J. Res. Dev. **30**, 397 (1986).
[62]T. Sakurai, T. Hashizume, I. Kamiya, Y. Hasegawa, A. Sakai, J. Matsui, E. Kono, T. Takahashi, and M. Ogawa, J. Vac. Sci. Technol. (in press, 1988).
[63]M. P. Cox and P. R. Griffin, J. Vac. Sci. Technol. A **6**, 376 (1988); this design is available commercially by VG Microscopes Limited, East Grinstead, England.
[64]S.-I. Park and C. F. Quate, Rev. Sci. Instrum. **58**, 2010 (1987).
[65]W. J. Kaiser and R. C. Jaklevic, Surf. Sci. **182**, L227 (1987).
[66]M. D. Pashley, K. W. Haberern, and W. Friday, J. Vac. Sci. Technol. A **6**, 488 (1988).
[67]B. Drake, R. Sonnenfeld, J. Schneir, P. K. Hansma, G. Slough, and R. V. Coleman, Rev. Sci. Instrum. **57**, 441 (1986).
[68]V. Elings and F. Wudl, J. Vac. Sci. Technol. A **6**, 412 (1988); this design is available commercially from Digital Instruments, Inc., Goleta, CA.
[69]A. P. Fein, J. R. Kirtley, and R. M. Feenstra, Rev. Sci. Instrum. **58**, 1806 (1987).
[70]J. G. H. Hermsen, H. van Kempen, B. J. Nelissen, L. L. Soethout, G. F. A. van der Walle, P. J. W. Weijs, and P. Wyder, Surf. Sci. **181**, 183 (1987).
[71]M. Salmeron, B. Marchon, S. Ferrer, and D. S. Kaufman, Phys. Rev. B **35**, 3036 (1987); this design is available from MacAllister Technical Services, Berkeley, CA.
[72]P. Davidsson, T. Claeson, and S. Pehrson, J. Vac. Sci. Technol. A **6**, 380 (1988).
[73]Commercially available design from W. A. Technology, Cambridge, England.
[74]P. Eustenberger, H. Rohrer, R. Christoph, and H. Siegenthaler, J. Electroanal. Chem. (in print, 1988).
[75]K. Besocke, Surf. Sci. **181**, 145 (1987).
[76]R. Guckenberger, C. Kosslinger, and W. Baumeister, J. Vac. Sci. Technol. A **6**, 383 (1988).
[77]L. Arnold, W. Krieger, and H. Walther, J. Vac. Sci. Technol. A **6**, 466 (1988).
[78]Y. Kuk, P. J. Silverman, H. Q. Nguyen, and P. H. Cutler (to be published).
[79]*Tunneling Spectroscopy*, edited by P. K. Hansma (Plenum, New York, 1982).
[80]S. A. Elrod, A. L. de Lozanne, and C. F. Quate, Appl. Phys. Lett. **45**, 1240 (1984).
[81]C. G. Slough, W. W. McNairy, R. V. Coleman, B. Drake, and P. K. Hansma, Phys. Rev. B **34**, 994 (1986).
[82]D. Eigler, Bull. Am. Phys. Soc. **32**, 542 (1987).
[83]H. Q. Nguyen, Ph.D. thesis, The Pennsylvania State University, 1988.
[84]F. M. Chua, Ph. D. thesis, Cambridge University, 1988.
[85]R. C. Dorf, *Modern Control System* (Addison–Wesley, Reading, MA, 1983).
[86]A. P. Sage and C. C. White, *Optimum System Control* (Prentice-Hall, Englewood Cliffs, NJ, 1977).
[87]M. Auguilar, P. J. Pascual, and A. Santisteba, IBM J. Res. Dev. **30**, 525 (1986).
[88]P. H. Schroer and J. Becker, IBM J. Res. Dev. **30**, 543 (1986).
[89]U. H. Bapst, Surf. Sci. **181**, 157 (1987).
[90]A. Bryant, D. E. P. Smith, and C. F. Quate, Appl. Phys. Lett. **48**, 832 (1986).
[91]L. W. Swanson and L. C. Crouser, J. Appl. Phys. **40**, 4741 (1969).
[92]H. W. Fink, IBM J. Res. Dev. **30**, 461 (1986).
[93]Y. Kuk, P. J. Silverman, and H. Q. Nguyen, J. Vac. Sci. Technol. A **6**, 524 (1988).
[94]R. S. Becker, J. A. Golovchenko, G. S. Higashi, and B. S. Swartzentruber, Phys. Rev. Lett. **57**, 1020 (1986).
[95]S.-I. Park and C. F. Quate, Appl. Phys. Lett. **48**, 112 (1986).
[96]R. Sonnenfeld and P. K. Hansma, Science **232**, 211 (1986).
[97]G. Binnig, C. F. Quate, and Ch. Gerber, Phys. Rev. Lett. **56**, 930 (1986).
[98]P. Muralt and D. W. Pohl, Appl. Phys. Lett. **48**, 514 (1986).
[99]U. Durig, D. W. Pohl, and F. Rohner, J. Appl. Phys. **59**, 3318 (1986).
[100]J. R. Matey and J. Blanc, J. Appl. Phys. **57**, 1437 (1985).

[101]W. J. Kaiser and L. D. Bell, Phys. Rev. Lett. **60**, 1406 (1988).
[102]D. W. Pohl and R. Moller, Rev. Sci. Instrum. **59**, 840 (1988).
[103]D. Tabor and R. H. S. Winterton, Proc. R. Soc. A **312**, 435 (1969).
[104]U. Durig, J. K. Gimzewski, and D. W. Pohl, Phys. Rev. Lett. **59**, 2403 (1986).
[105]C. M. Mate, G. M. McClelland, R. Erlandsson, and S. Chiang, Phys. Rev. Lett. **59**, 1942 (1987).
[106]Y. Martin, C. C. Williams, and H. K. Wickeramasinghe, J. Appl. Phys. **61**, 4723 (1987).
[107]O. Marti, B. Drake, and P. K. Hansma, Appl. Phys. Lett. **51**, 484 (1987).
[108]G. Binnig, Ch. Gerber, E. Stoll, T. R. Albrecht, and C. F. Quate, Europhys. Lett. **3**, 1281 (1987).
[109]R. Yang, R. Miller, and P. J. Bryant, J. Appl. Phys. **63**, 570 (1988).
[110]T. R. Albrecht and C. F. Quate, J. Appl. Phys. **62**, 2599 (1987).
[111]G. M. McClelland, R. Erlandsson, and S. Chiang, *Review of Progress in Quantitative Non-Destructive Evaluation*, edited by D. O. Thompson and D. E. Chimenti (Plenum, New York, 1987), Vol. 6 B, pp. 1307–1314.
[112]P. Muralt, H. Meiser, D. W. Pohl, and H. W. M. Salemink, Appl. Phys. Lett. **50**, 1352 (1987).
[113]J. R. Kirtley, S. Washburn, and M. J. Brady, Phys. Rev. Lett. **60**, 1546 (1988).
[114]E. A. Ash and G. Nicholas, Nature **237**, 510 (1972).
[115]U. Ch. Fischer and H. P. Zingsheim, Appl. Phys. Lett. **40**, 195 (1982).
[116]A. Lewis, M. Isaacson, H. Harootunian, and A. Murray, Ultramicroscopy **13**, 227 (1984).
[117]R. S. Becker, J. A. Golovchenko, E. G. McRae, and B. S. Swartzentruber, Phys. Rev. Lett. **55**, 2028 (1985).
[118]R. J. Hamers, R. M. Tromp, and J. E. Demuth, Phys. Rev. Lett. **56**, 1972 (1986).
[119]R. M. Tromp, R. J. Hamers, and J. E. Demuth, Phys. Rev. B **34**, 1388 (1986).
[120]Th. Berhaus, A. Brodde, H. Neddermeyer, and St. Tosch, J. Vac. Sci. Technol. A **6**, 483 (1988).
[121]K. Takayanagi, Y. Tanishiro, M. Takahashi, and S. Takahashi, J. Vac. Sci. Technol. A **3**, 1502 (1985).
[122]R. M. Tromp, R. J. Hamers, and J. E. Demuth, Phys. Rev. Lett. **55**, 1303 (1985); R. J. Hamers, R. M. Tromp, and J. E. Demuth, Phys. Rev. B **34**, 5543 (1986).
[123]R. S. Becker, B. S. Swartzentruber, and J. S. Vickers, J. Vac. Sci. Technol. A **6**, 478 (1988).
[124]Th. Berghaus, A. Brodde, H. Neddermeyer, and St. Tosch, J. Vac. Sci. Technol. A **6**, 478 (1988).
[125]J. A. Stroscio, R. M. Feenstra, and A. P. Fein, Phys. Rev. Lett. **57**, 2579 (1986); J. Vac. Sci. Technol. A **5**, 838 (1987).
[126]J. A. Stroscio, R. M. Feenstra, and A. P. Fein, Phys. Rev. Lett. **58**, 1668 (1987).
[127]R. J. Wilson and S. Chiang, Phys. Rev. Lett. **58**, 369 (1987); Phys. Rev. Lett. **59**, 2329 (1987).
[128]E. J. van Loenen, J. E. Demuth, R. M. Tromp, and R. J. Hamers, Phys. Rev. Lett. **58**, 373 (1987).
[129]R. J. Wilson and S. Chiang, Phys. Rev. Lett. **58**, 2575 (1987).
[130]R. J. Hamers and J. E. Demuth, J. Vac. Sci. Technol. A **6**, 512 (1988).
[131]R. S. Becker, B. S. Swatzentruber, J. S. Vickers, M. S. Hybertsen, and S. G. Louie, Phys. Rev. Lett. **60**, 116 (1988).
[132]J. Nogami, S.-I. Park, and C. F. Quate, Phys. Rev. B **36**, 6221 (1987).
[133]G. Binnig, H. Rohrer, Ch. Gerber, and E. Weibel, Surf. Sci. **131**, L379 (1983).
[134]H. Q. Nguyen, Y. Kuk, and P. J. Silverman, J. Phys. (to be published, 1989).
[135]V. M. Hallmark, S. Chiang, J. F. Rabolt, J. D. Swalen, and R. J. Wilson, Phys. Rev. Lett. **59**, 2879 (1987).
[136]Y. Kuk, P. J. Silverman, and M. F. Jarrold (to be published).
[137]Y. Kuk, P. J. Silverman, and H. Q. Nguyen, Phys. Rev. Lett. **59**, 1452 (1987).
[138]R. J. Behm, W. Hosler, E. Ritter, and G. Binnig, Phys. Rev. Lett. **56**, 228 (1986); E. Ritter, R. J. Behm, G. Potschke, and J. Wintterlin, Surf. Sci. **181**, 403 (1987).
[139]B. Marchon, P. Bernhardt, M. E. Bussell, G. A. Somorjai, M. Salmeron, and W. Siekhaus, Phys. Rev. Lett. **60**, 1166 (1988).
[140]Y. Kuk, P. J. Silverman, and T. M. Buck, Phys. Rev. B **36**, 2863 (1987).
[141]P. K. Hansma, Bull. Am. Phys. Soc. **30**, 251 (1985).
[142]R. V. Coleman, B. Drake, P. K. Hansma, and G. Slough, Phys. Rev. Lett. **55**, 394 (1985).
[143]G. Binnig, H. Fuchs, Ch. Gerber, H. Rohrer, E. Stoll, and E. Tosattis, Europhys. Lett. **1**, 31 (1986).
[144]H. J. Mamin, E. Ganz, D. W. Abraham, R. E. Thomson, and J. Clarke, Phys. Rev. B **34**, 9015 (1986).
[145]J. M. Soller, A. M. Baro, N. Garcia, and H. Rohrer, Phys. Rev. Lett. **57**, 444 (1986).
[146]More papers were published in the Proceedings of the 1st and 2nd International Conference on STM, Surf. Sci. **181** (March, 1987); J. Vac. Sci. Technol. A **6** (March/April, 1988).
[147]B. Giambattista, A. Johnson, R. V. Coleman, B. Drake, and P. K. Hansma, Phys. Rev. B **37**, 2741 (1988); B. Giambattista, A. Johnson, W. W. McNairy, C. G. Slough, and R. V. Coleman (to be published).
[148]T. Sleator and R. Tycko, Phys. Rev. Lett. **60**, 1418 (1988).
[149]M. Amrein, A. Stasiak, H. Gross, E. Stoll, and G. Travaglini, Science **240**, 514 (1988).
[150]J. K. Gimzewski, E. Stoll, and R. R. Schlittler, Surf. Sci. **181**, 267 (1987).
[151]R. Guckenberger, C. Kosslinger, R. Gatz, H. Breu, N. Levin, and W. Baumeister, Ultramicroscopy (to be published).
[152]J. Schneir and P. K. Hansma (private communication).
[153]J. S. Foster and J. E. Frommer, Nature (to be published).
[154]M. Gerhrtz, H. Strecker, and H. Grim, J. Vac. Sci. Technol. A **6**, 432 (1988).
[155]N. Garcia, A. M. Baro, R. Garcia, J. P. Pena, and H. Rohrer, Appl. Phys. Lett. **47**, 367 (1985).
[156]S. Okayama, M. Komino, W. Mizutani, H. Tokumoto, M. Okano, K. Shimizu, Y. Kobayashi, F. Matsumoto, S. Wakiyama, M. Shigeno, F. Sakai, S. Fujiwara, O. Kitamina, M. Ono, and K. Kajimura, J. Vac. Sci. Technol. A **6**, 440 (1988).
[157]M. A. McCord and R. F. W. Pease, Appl. Phys. Lett. **50**, 569 (1987).
[158]U. Staufer, R. Wiesendanger, L. Eng, L. Rosenthaler, H. R. Hidber, H.-J. Guntherodt, and N. Garcia, Appl. Phys. Lett. **51**, 244 (1987).
[159]R. C. Jaklevic and L. Elie, Phys. Rev. Lett. **60**, 120 (1988).
[160]R. S. Becker, J. A. Golovchenko, and B. S. Swartzentruber, Nature **325**, 419 (1987).
[161]B. Drake, R. Sonnenfeld, J. Schneir, and P. K. Hansma, Surf. Sci. **181**, 92 (1987).